NASA CR-132617

IMPROVEMENTS TO THE SADSAM COMPUTER PROGRAM FOR AEROELASTICITY ANALYSIS

By Robert G. Schwendler

March 1975

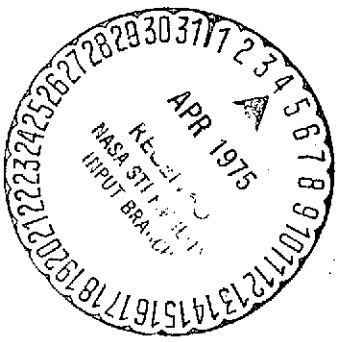

Prepared under Contract No. NAS1-12017

By The MacNeal-Schwendler Corporation
Los Angeles, California

for

NATIONAL AERONAUTICS AND SPACE ADMINISTRATION

(NASA-CR-132617) IMPROVEMENTS TO THE SADSAM COMPUTER PROGRAM FOR AEROELASTICITY ANALYSIS (MacNeal-Schwendler Corp.) 29 p HC $3.75 CSCL 01A
N75-19173
Unclas
G3/02 13380

TABLE OF CONTENTS

Section	Page
INTRODUCTION	1
EIGENVECTOR NORMALIZATION	2
COMPLEX EIGENVECTOR FORCES & ENERGY DISTRIBUTION	2
MODAL COMPOSITION OF EIGENVECTORS	3
DETERMINATION OF RIGID BODY MODES	3
REVISED AERODYNAMIC FORCE REPRESENTATION	3
Flap Aerodynamics	4
Chordwise Motions and Aerodynamic Forces	8
Wing-Tail Interaction	12
GUST ANALYSIS	13
REFERENCES	18
APPENDIX A - Aircraft Configuration Used in Sample Gust Analysis	

List of Tables and Illustrations

Figure 1. Coordinate Systems	14
Table 1. Notation	15
Table 2. W Functions	17

IMPROVEMENTS TO THE SADSAM COMPUTER PROGRAM FOR AEROELASTICITY ANALYSIS*

INTRODUCTION

This report contains a summary description of the work accomplished under NASA contract NAS1-12017. In general the work includes enhancements in the capability and efficiency of the SADSAM computer program at LRC and illustrative analyses demonstrating gust analysis capabilities of SADSAM.

The modifications to the SADSAM computer program included:

1. Incorporation of 3 optional methods of normalization for normal mode shapes and complex eigenvectors.
2. The addition of the capability to determine the element and aerodynamic forces from complex eigenvectors.
3. The addition of the capability to determine the element and aerodynamic energy distribution from complex eigenvectors.
4. The addition of the capability to determine the modal composition of of complex eigenvectors.
5. The addition of the capability to determine zero frequency (rigid body) normal mode shapes.
6. Enhancement of the aerodynamic formulation by the addition of provisions for control surfaces, wing downwash effects on tail surfaces, chordwise displacement and chordwise forces.
7. The improvement of the efficiency of transient analysis.
8. Miscellaneous corrections and convenience improvements.

Appendices attached to this report were prepared for the "Theoretical Basis of the SADSAM Computer Program." The numbering of these appendices is consistent with that document and therefore results in numbering gaps in this report.

* The contract research effort which has lead to the results in this report was financially supported by USAAMRDL (Langley Directorate).

EIGENVECTOR NORMALIZATION

Prior to the SADSAM program modification under this contract, normal mode shapes were normalized to a unit generalized mass and complex eigenvectors were normalized to unity at the maximum displacement magnitude.

At the user's option complex eigenvectors also can now be normalized to an effective unit generalized mass as defined by equation D-2 of appendix D. Provision has been made, through the use of the ØMITGENM data card, to omit selected degrees of freedom from the calculation of the "generalized mass" of complex eigenvectors. This provision is made so that non-structural masses, such as those associated with lag functions, may be excluded from the calculation of "generalized mass."

Also at the user's option either normal mode shapes or complex eigenvectors can be normalized to a unit value at the degree of freedom having the maximum displacement magnitude or a user selected degree of freedom.

COMPLEX EIGENVECTOR FORCES & ENERGY DISTRIBUTION

The SADSAM program has had the capability of calculating the elastic element forces and strain energy distribution for normal mode shapes. The program modifications made under this effort extend this capability to complex eigenvectors.

The definition of force and energy distribution of a complex eigenvector is more comprehensive than in the real case since it includes the consideration of mass elements, damper elements, and aerodynamic forces as well as the elastic elements included for the normal mode shapes. Appendix D contains a derivation and discussion of the complex force and "complex energy" calculated for complex eigenvectors.

MODAL COMPOSITION OF EIGENVECTORS

Flutter analyses are made by SADSAM in terms of the physical coordinates of the system. In many cases insight into a flutter phenomenon can be gained through the examination of the normal mode components of the complex eigenvector associated with the flutter root. For these purposes the capability of calculating modal components of complex eigenvectors was added to the SADSAM program.

A derivation and discussion of the method used is contained in appendix D.

DETERMINATION OF RIGID BODY MODES

Analyses of free systems which included rigid body modes has always been within the capability of SADSAM. In the determination of normal modes of free systems, only the finite frequency modes were calculated. In order to fully exploit the new capability to determine modal composition, it was necessary to add the ability to calculate rigid body mode shapes. A derivation and discussion of the method used is contained in appendix F.

REVISED AERODYNAMIC FORCE REPRESENTATION

One of the development tasks has been to extend SADSAM's existing capability for representing aerodynamic forces on a swept-back lifting surface. The existing capability is described in Appendix C of the SADSAM Theoretical Manual. In the existing capability, the lifting surface is treated as a structural beam with out-of-plane bending and torsional degrees of freedom. The aerodynamic forces include lift and moment about a structural reference axis. They are computed according to a modified strip theory which permits the user to specify the center

of pressure, the lift curve shape, and the lag function parameters for each strip. He can also specify a gust function. The calculations are performed in either the time domain or in the frequency domain at the user's option. Flutter analysis is performed by the p-method, using SADSAM's standard complex eigenvalue extraction technique. This method has the advantages that the computed decay rates are realistic, and that results are obtained for each specific speed without recourse to interpolation, as would be required by the more commonly used reduced frequency method.

The extensions which have been implemented include:

a. Addition of degrees of freedom to represent, at each strip, a sealed flap without aerodynamic overhang.

b. Inclusion of chordwise aerodynamic forces and a chordwise degree of freedom for each strip. The intended purpose of this extension is to permit the analysis of low frequency rigid body modes (e.g., phugoid motion) as well as the analysis of lifting surfaces with low chordwise rigidity.

c. Representation of wing-induced downwash on tail surfaces (or canard-induced downwash on wing and tail surfaces), including time delay due to convection.

The theory for each of these effects will be described separately.

Flap Aerodynamics

Unsteady aerodynamic forces for an airfoil with flap in an incompressible, two-dimensional flow are derived in Theodorsen's classical paper, Ref. 1. The assumptions made in that paper regarding flap geometry - namely that the gap is sealed and that the flap leading edge coincides with the hinge line - are also assumed here. Summaries of the equations

and of the notation used by various authors will be found in textbooks, for example, Ref. 2. We prefer to use the notation developed by Wilts, Ref. 3, who clearly differentiates the physical origins of the terms.

The airplane geometry and the associated coordinate systems are shown in Figure 1. The "reference axis" makes an angle Λ with the aircraft's y_a axis and lies at a distance x_{ref} behind the leading edge of the lifting surface. x_{ref} is measured perpendicular to the reference axis. x, z, θ, and β are structural degrees of freedom defined at a point on the reference axis. Aerodynamic forces and moments are applied to these same degrees of freedom. The flap hinge is parallel to the reference axis at a distance x_h from the leading edge. The angular motion of the flap relative to the non-rotating part of the airfoil is δ. The positive direction of rotation is shown in Figure 1. The chord, c, and the spanwise dimension of the strip, Δr, are measured perpendicular and parallel to the reference axis, respectively.

The equations for the aerodynamic pitching moment, M_θ, lift, P_z, and hinge moment, M_δ, all measured in the positive coordinate directions, are

$$\begin{Bmatrix} M_\theta \\ F_z \\ M_\delta \end{Bmatrix} = \tfrac{1}{2}\rho\bar{V}^2 c\Delta r \left(C_{\ell\alpha} \begin{Bmatrix} x_{ref}-x_p \\ 1 \\ cw_3 \end{Bmatrix} (C(s)\alpha_{rot} + \psi(s)\alpha_{gust}) \right.$$

$$\left. - \begin{Bmatrix} \frac{\pi c}{8} w_4 \\ 0 \\ \frac{\pi c}{8} w_7 \end{Bmatrix} \delta - \frac{\pi c}{2\bar{V}} [A_1] \begin{Bmatrix} \dot{\theta} \\ \dot{z} \\ \dot{\delta} \end{Bmatrix} - \frac{\pi c}{2\bar{V}^2} [A_2] \begin{Bmatrix} \ddot{\theta} \\ \ddot{z} \\ \ddot{\delta} \end{Bmatrix} \right) \qquad (1)$$

The notation used in Equation 1 is defined in Table 1. The velocity

$$\bar{V} = V \cos \Lambda \tag{2}$$

is the component of free-stream velocity perpendicular to the reference axis. The first term within brackets is the contribution of circulation and the remaining terms are respectively the noncirculatory stiffness, damping and apparent mass terms. The coefficient matrices in the apparent damping and mass terms are

$$[A_1] = \begin{bmatrix} -(x_p - x_{ref})\frac{C_{\ell\alpha}}{2\pi} & 0 & c\left(\frac{w_5}{4} + w_{11}\right) + (x_h - x_{ref})w_9 \\ \frac{C_{\ell\alpha}}{2\pi} & 0 & -w_9 \\ c\left(\frac{w_6}{4} + w_{10}\right) & 0 & c\left(\frac{w_8}{4} + w_{13}\right) \end{bmatrix} \tag{3}$$

$$[A_2] = \begin{bmatrix} \frac{c^2}{32} + \left(x_{ref} - \frac{c}{2}\right)^2 & x_{ref} - \frac{c}{2} & c^2 w_{12} + c(x_h - x_{ref})w_{10} \\ x_{ref} - \frac{c}{2} & 1 & -cw_{10} \\ c^2 w_{12} + c(x_h - x_{ref})w_{10} & -cw_{10} & c^2 w_{14} \end{bmatrix} \tag{4}$$

The angle of attack due to motion at the rotation center, α_{rot}, is the following function of the motions of the strip

$$\alpha_{rot} = \theta + \tan \Lambda \beta + w_1 \delta - \frac{1}{\bar{V}} \left(\dot{z}_{ref} - (c - x_p - x_{ref})\dot{\theta} - cw_2\dot{\delta}\right) \tag{5}$$

The angle of attack due to gust is

$$\alpha_{gust} = \frac{U(t-\tau)}{\bar{V}} \tag{6}$$

where $U(t-\tau)$ is the vertical gust velocity delayed by a time, τ, which is specified independently for each strip. The coefficients w_i $i = 1, 2, ---, 14$ are functions of the hinge location, x_h/c. They are closely related to Küssner's Φ functions, Ref. 4. Formulas for the coefficients are listed in Table 2. The user will have the option in SADSAM to specify his own values of the coefficients. It is possible that some of the coefficients may be available from test data. For example, w_1, w_3, w_4 and w_7 can be obtained from static tests in a wind tunnel.

$C(s)$ and $\psi(s)$, where $s = cp/2\bar{V}$, are respectively the Theodorsen and Küssner functions. They are approximated in SADSAM by the following bi-quadratic polynomial fractions

$$C(s) = \frac{(1 + d_1 s)(1 + d_3 s)}{(1 + d_2 s)(1 + d_4 s)} \tag{7}$$

$$\psi(s) = \frac{1 + d_5 s}{(1 + d_6 s)(1 + d_7 s)} \tag{8}$$

The user has the option to select his own values of the coefficients d_1 to d_7. The following default values have been shown to be good approximations for the two-dimensional incompressible case, Ref. 3.

$d_1 = 10.61$ $\quad d_3 = 1.774$ $\quad d_5 = 6.608$ $\quad d_7 = .834$

$d_2 = 13.51$ $\quad d_4 = 2.745$ $\quad d_6 = 10.0$

Chordwise Motions and Aerodynamic Forces

Chordwise motions and aerodynamic forces are important for the aeroelastic analysis of fixed wing aircraft when low frequency stability and control characteristics are a consideration. They are important for rotary wing aircraft because the lower chordwise vibration modes occur in the same frequency range as the lower flapwise bending modes. This situation can also occur for some types of fixed wings.

The coordinate geometry that will be used is shown in Figure 1. The x-direction is perpendicular to the reference axis. The following sketch shows the assumed flow condition in the x-z plane.

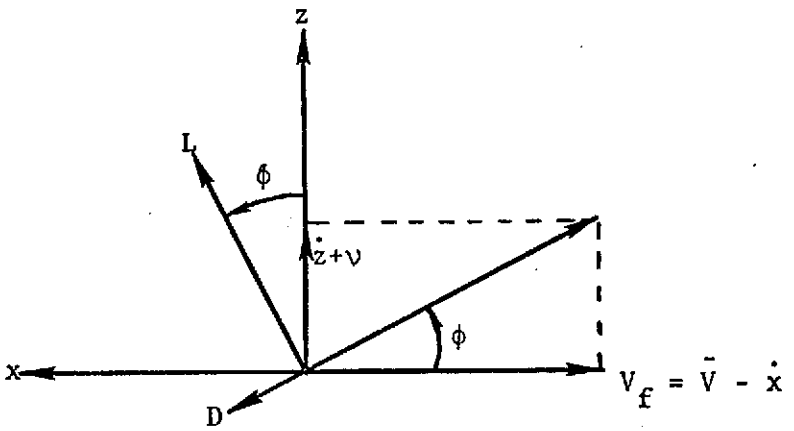

In the sketch, $\bar{V}$ is the component of the airplane's velocity relative to the free stream which is normal to the reference axis, and ν is the induced velocity. For small angles, it may be assumed that the chordwise force on the strip is

$$F_x = D + L\phi \tag{9}$$

where D is the profile drag,

$$D = \tfrac{1}{2}\rho V_f^2 c \Delta r \cdot C_D \ , \tag{10}$$

L is the lift,

$$L = \tfrac{1}{2}\rho V_f^2 c \Delta r \cdot C_L \ , \tag{11}$$

and ϕ is the inflow angle,

$$\phi = \frac{\dot{z} + v}{V_f} = \frac{\dot{z}}{V_f} + \alpha_{ind} \ . \tag{12}$$

According to elementary momentum theory, Ref. 5, the induced angle of attack

$$\alpha_{ind} = C_L/\pi A \tag{13}$$

where A is the aspect ratio of the surface. The induced angle of attack reduces the angle between the flow and the chord plane, so that, assuming a linear relationship between lift and angle of attack,

$$C_L = C_{\ell\alpha}^{\infty}(\alpha - \alpha_{ind}) \ , \tag{14}$$

where $C_{\ell\alpha}^{\infty}$ is the lift curve slope for two-dimensional flow. Elimination of α_{ind} between Equations 13 and 14 gives

$$C_L = \left(\frac{C_{\ell\alpha}^{\infty}}{1 + \frac{C_{\ell\alpha}^{\infty}}{\pi A}} \right) \alpha \tag{15}$$

so that the lift curve slope including aspect ratio correction is

$$C_{\ell\alpha} = \frac{C_{\ell\alpha}^{\infty}}{1 + \frac{C_{\ell\alpha}^{\infty}}{\pi A}} \tag{16}$$

Also, from Equation 14,

$$\alpha_{ind} = \left(1 - \frac{C_{\ell\alpha}}{C_{\ell\alpha}^{\infty}} \right) \alpha = \frac{C_{\ell\alpha}}{\pi A} \cdot \alpha \tag{17}$$

We are now prepared to write expressions for the forces in the z and x directions. Assuming ϕ small and ignoring the small contribution of drag in the z direction

$$F_z = L = \tfrac{1}{2}\rho V_f^2 c\Delta r\, C_{\ell\alpha}\cdot\alpha \tag{18}$$

The forward velocity includes the dynamic perturbation $\dot{x}$, i.e.,

$$V_f = \bar{V} - \dot{x} \tag{19}$$

while the angle of attack, which includes both a steady part θ_0 and a dynamic part, is

$$\alpha = \theta_0 + C(s)\alpha_{rot} + \psi(s)\alpha_{gust} \tag{20}$$

where α_{rot}, α_{gust}, $C(s)$ and $\psi(s)$ are obtained from Equations 5, 6, 7 and 8, respectively. Note that the steady part of α_{ind} is accounted for in the calculation of $C_{\ell\alpha}$ and should not, therefore, be subtracted from θ_0. In the expressions for α_{rot} and α_{gust} the velocity $\bar{V}$ should be replaced by V_f, but the effect of the substitution is second order small and will be neglected. If the lift is separated into a steady part L_0 and a dynamic perturbation δL, then Equations 18 to 20 give

$$L_0 = \tfrac{1}{2}\rho\bar{V}^2 c\Delta r\, C_{\ell\alpha}\theta_0 \tag{21}$$

and

$$\delta F_z = \delta L = \tfrac{1}{2}\rho\bar{V}^2 c\Delta r\, C_{\ell\alpha}\left(C(s)\alpha_{rot} + \psi(s)\alpha_{gust} - 2\theta_0\frac{\dot{x}}{\bar{V}}\right) + \text{(nonlinear terms)} \tag{22}$$

The nonlinear terms will be neglected. The chordwise force given by Equation 9 can similarly be separated into a steady part and a dynamic perturbation. The dynamic perturbation is

$$\delta F_x = \delta D + L_0 \delta\phi + \phi_0 \delta L \tag{23}$$

L_0 and δL are given by Equations 21 and 22. In addition,

$$\delta D = -\tfrac{1}{2}\rho \bar{V}^2 c \Delta r C_D \cdot \frac{2\dot{x}}{\bar{V}} \tag{24}$$

$$\phi_0 = \frac{C_{\ell\alpha}}{\pi A} \theta_0 \tag{25}$$

and

$$\delta\phi = \frac{\dot{z}}{\bar{V}} + \frac{C_{\ell\alpha}}{\pi A} \left(C(s)\alpha_{rot} + \psi(s)\alpha_{gust}\right) \tag{26}$$

Substitution into Equation 23 gives

$$\delta F_x = \tfrac{1}{2}\rho \bar{V}^2 c \Delta r \left[\frac{2C_{\ell\alpha}^2 \theta_0}{\pi A} \left(C(s)\alpha_{rot} + \psi(s)\alpha_{gust}\right) + C_{\ell\alpha}\theta_0 \frac{\dot{z}}{\bar{V}} - 2\left(C_D + \frac{(C_{\ell\alpha}\theta_0)^2}{\pi A}\right) \frac{\dot{x}}{\bar{V}} \right] \tag{27}$$

Equations 22 and 27 are used to generate perturbation aerodynamic forces for SADSAM. The perturbation pitching moment and hinge moment are obtained by multiplying δF_z by $x_{ref}-x_p$ and cw_3 respectively, as in Equation 1.

One further refinement is that the structural x and z axes may be rotated out of the aircraft's x_a, y_a plane through an angle γ about the pitch axis. Thus, the forces applied to the structure are related to the forces computed in Equations 22 and 27 by

$$\begin{Bmatrix} F_z \\ F_x \end{Bmatrix} = \begin{bmatrix} \cos\gamma & \sin\gamma \\ -\sin\gamma & \cos\gamma \end{bmatrix} \begin{Bmatrix} \delta F_z \\ \delta F_x \end{Bmatrix} \tag{28}$$

while the velocities appearing in the equations are related to the structural velocities by

$$\begin{Bmatrix} \dot{z} \\ \dot{x} \end{Bmatrix} = \begin{bmatrix} \cos\gamma & -\sin\gamma \\ \sin\gamma & \cos\gamma \end{bmatrix} \begin{Bmatrix} \dot{\bar{z}} \\ \dot{\bar{x}} \end{Bmatrix} \tag{29}$$

The additional parameters required to describe the effects treated in this section are:

θ_0, the steady angle of incidence of the lifting surface, relative to the free stream, which may be different for each strip,

C_D, the drag coefficient,

A, the aspect ratio,

γ, the rotation angle of the structural x and z axes, which may be different for each strip.

Wing-Tail Interaction

A lifting surface will induce an angle of attack on a lifting surface in its wake. This effect is important for the analysis of the response to gusts. The induced angle of attack can be expressed in the form

$$\alpha_{it} = -\left(\frac{\partial \varepsilon_t}{\partial C_{\ell w}}\right) C_{\ell w}(t-\tau) \tag{30}$$

where ε_t is the induced flow angle (positive downward) at the tail, and $C_{\ell w}(t-\tau)$ is the lift coefficient at some representative station on the wing, delayed by the time increment required for the wake to be convected from the wing to the tail. The dynamic part of α_{it} will be included in the expression for angle of attack, Equation 5, for all affected tail strips, but the steady part will be ignored. (The user can include the steady part in θ_0, if he wishes.)

GUST ANALYSIS

A gust analysis was made of a hypothetical small aircraft to demonstrate the gust analysis capability of SADSAM. The definition of the aircraft configuration and the analyses were accomplished cooperatively with the contract monitor.

Appendix A contains a definition of the aircraft configuration and a summart of some of the results of the analysis.

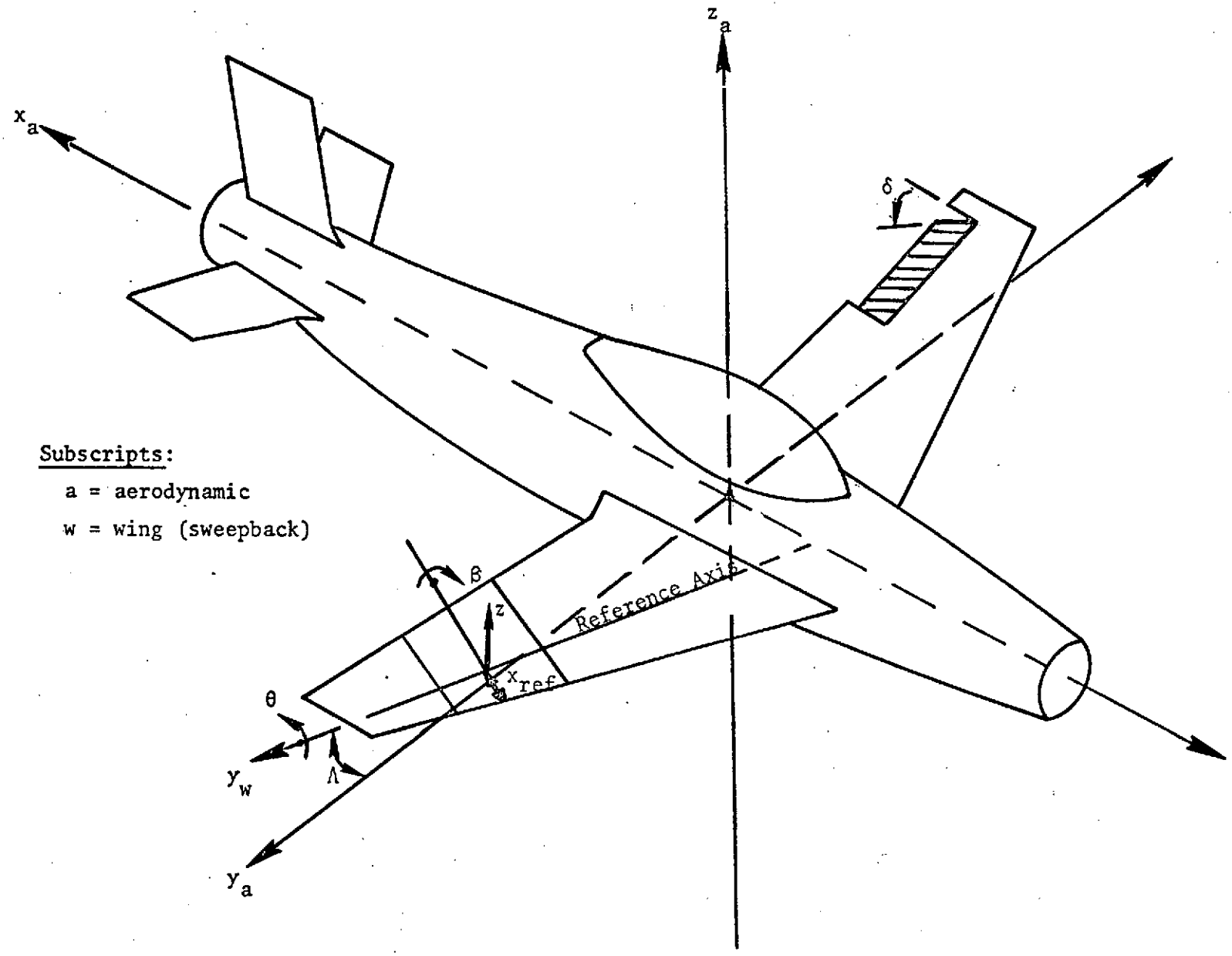

Figure 1. Coordinate Systems

Table 1. Notation

c	chord
s	$cp/2\bar{V}$, complex form of reduced frequency
t	time
$w_1, w_2, \ldots, w_{14}$	see Table 2
x	chordwise coordinate, see Figure 1 for positive direction
x_h	distance from leading edge to hinge line
x_p	distance from leading edge to center of pressure
x_{ref}	distance from leading edge to reference axis
z	vertical coordinate, see Figure 1 for positive direction
A	aspect ratio
C_D	drag coefficient
C_L	lift coefficient
$C_{\ell\alpha}$	lift curve slope
$C^{\infty}_{\ell\alpha}$	lift curve slope for two-dimensional flow
$C_{\ell w}$	lift coefficient at some point on the wing
$C(s)$	Theodorsen's function
D	drag
F_x	chordwise aerodynamic force
F_z	vertical aerodynamic force
L	lift
L_0	steady part of lift
M_δ	hinge moment
M_θ	pitching moment
$U(t-\tau)$	vertical gust velocity at a particular strip
V	free stream velocity
$\bar{V}$	component of free-stream velocity normal to the reference axis

Table 1. Notation (Continued)

V_f	$\bar{V} - \dot{x}$
α	angle of attack
α_{gust}	angle of attack due to gust
α_{ind}	induced angle of attack
α_{it}	induced angle of attack at the tail due to lift on the wing
α_{rot}	angle of attack at the rotation center
β	spanwise slope, see Figure 1 for positive direction
γ	rotation angle of the structural axes relative to the aerodynamic axes
δ	relative flap angle, see Figure 1 for positive direction
δD	dynamic part of drag
δF_z	dynamic part of F_z
δL	dynamic part of lift
$\delta\phi$	dynamic part of ϕ
ϵ_t	induced flow angle at the tail
θ	pitch angle, see Figure 1 for positive direction
θ_0	steady angle of incidence relative to the free stream
ν	induced velocity
ρ	air density
τ	time delay due to convection
ϕ	inflow angle, see Equation 12
ϕ_0	steady part of ϕ
$\psi(s)$	Küssner's function
Δr	spanwise width of strip
Λ	sweep-back angle

Table 2. W Functions

Note: $\phi = \cos^{-1}\left(\frac{2x_h}{c} - 1\right)$

$$W_1 = \frac{1}{\pi}\left[\phi + \sin\phi\right]$$

$$W_2 = \frac{1}{4\pi}\left[\sin\phi\,(2 - \cos\phi) + \phi(1 - 2\cos\phi)\right]$$

$$W_3 = \frac{1}{4\pi}\left[\sin\phi\,(2 + \cos\phi) - \phi(1 + 2\cos\phi)\right]$$

$$W_4 = \frac{4}{\pi}\left[\sin\phi\,(1 + \cos\phi)\right]$$

$$W_5 = \frac{1}{\pi}\left[\phi + \frac{1}{3}(\sin\phi)(2 + \cos\phi)(1 - 2\cos\phi)\right]$$

$$W_6 = \frac{1}{\pi}\left[\phi - \frac{1}{3}(\sin\phi)(2 - \cos\phi)(1 + 2\cos\phi)\right]$$

$$W_7 = \frac{4}{\pi^2}\left[\sin\phi\,(1 + \cos\phi)(\phi - \sin\phi)\right]$$

$$W_8 = \frac{1}{\pi^2}\left[\sin\phi\cos\phi - \phi\right]^2$$

$$W_9 = \frac{1}{\pi}\left[-\sin\phi\cos\phi + \phi\right]$$

$$W_{10} = \frac{1}{2\pi}\left[-\phi\cos\phi + \frac{1}{3}\sin\phi\,(2 + \cos^2\phi)\right]$$

$$W_{11} = \frac{1}{2\pi}\left[-\phi\cos\phi + \frac{1}{3}\sin\phi\,(1 + 2\cos^2\phi)\right]$$

$$W_{12} = \frac{1}{4\pi}\left[\phi\left(\frac{1}{8} + \cos^2\phi\right) - \frac{1}{8}(7 + 2\cos^2\phi)\sin\phi\cos\phi\right]$$

$$W_{13} = \frac{1}{2\pi^2}\left[-\phi\cos\phi + \sin\phi\right]\left[\phi - \cos\phi\sin\phi\right]$$

$$W_{14} = \frac{1}{4\pi^2}\left[\phi^2\left(\frac{1}{8} + \cos^2\phi\right) - \frac{1}{4}\phi\sin\phi\cos\phi(7 + 2\cos^2\phi) + \frac{1}{8}\sin^2\phi(4 + 5\cos^2\phi)\right]$$

REFERENCES

1. Theodorsen, T., "General Theory of Aerodynamic Instability and the Mechanism of Flutter," NACA TR-496, 1934.

2. Scanlan, R. H., and Rosenbaum, R., Introduction to the Study of Aircraft Vibration and Flutter, The MacMillan Co., N.Y., 1951.

3. Wilts, C. H., "Aerodynamic Forces in Analog Computation," California Institute of Technology, Computing Center, Technical Report No. 116, September, 1959.

4. Küssner, H. G., "Zusammenfassender Bericht über instationären Auftrieb von Flugeln," Luftfahrt-Forsch., 13, 412-424, 1936.

5. Perkins, C. D., and Hage, R. E., Airplane Performance Stability and Control, John Wiley & Sons, Inc., N.Y., 1954.

APPENDIX A

Aircraft Configuration Used in Sample Gust Analysis

Wing:

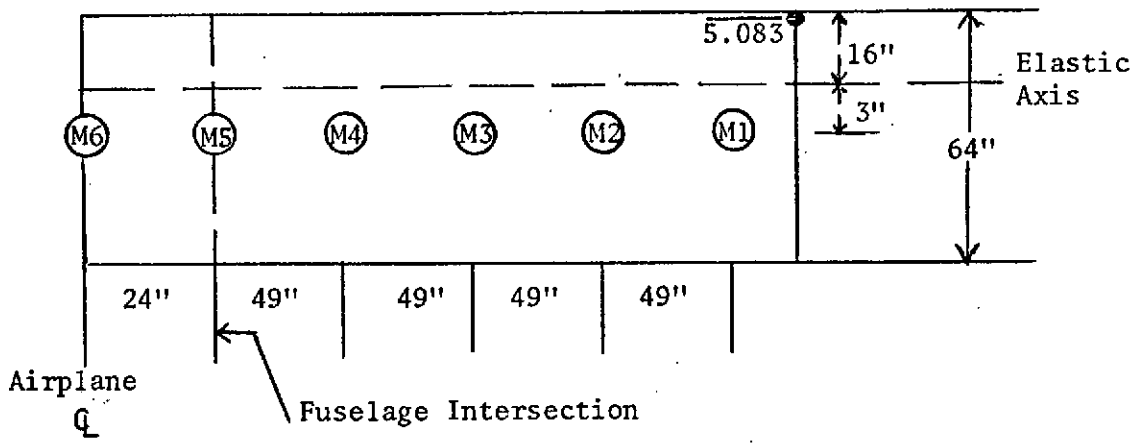

Wing Stiffness

$GJ = EI = 49 \times 10^7$ LB.IN^2

Wing Mass

Sta. In.	Empty Wing		Fuel	
	MASS LB.SEC^2/IN.	PITCH INERTIA LB.SEC^2/IN.	MASS	PITCH INERTIA
0	.01295	3.315	0	0
24	.0578	14.80	.1166	0
73	.08971	22.97	.2332	0
122	.08971	22.97	.1166	0
171	.08971	22.97	0	0
220	.04485	11.48	0	0

All Wing Mass CG 19" Aft of L.E.

Horizontal Tail:

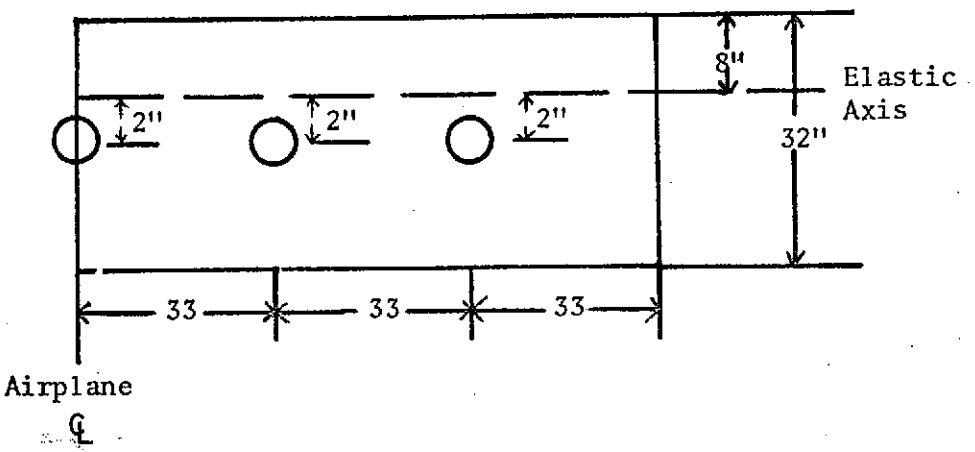

Stiffness:

$$EI = GJ = 3.07 \times 10^{7} \text{ LB.IN}^2$$

Mass:

Sta In.	Mass LB.SEC^2/IN.	Pitch Inertia LB.SEC^2/IN.
0	.0095	.608
33	.0190	1.216
66	.0190	1.216
99	.0207	.608

Horizontal tail rotation about the 1/4 chord is restrained by a spring (k) connected to the fuselage slope at Sta. 17, where:

$$k = 1.18 \times 10^{5} \text{ in.lb/rad}$$

1/2 Fuselage:

Sta.		Mass (lb.sec^2/in) Empty	Mass (lb.sec^2/in) Load	Stiffness EI (lb.in^2) Linear between Points
-16		.7617	.0285	4.62×10^8
17		.3135	.1632	4.62×10^8 5×10^9
47	Wing ¼ chord	.3277	.4741	5×10^9
90		.1736	.3446	5×10^9 3.35×10^9
130		.0531	0	1.655×10^9
175		.0311	0	5.75×10^8
220	Horiz.Tail ¼ chord	.0453	0	1.00×10^8

SAS

Horizontal Tail Rotation (δ_t) due to Pitch ($\dot{\theta}$)

$$\delta_t(\text{deg}) = k_{\dot{\theta}}\left(\frac{2}{\bar{s}+2}\right)\left(\frac{30}{\bar{s}+30}\right)\dot{\theta}\,(\text{deg/sec})$$

$$s = \frac{\bar{s}}{3}$$

$$\frac{\delta_t}{\theta} = \frac{k_{\dot{\theta}} s}{(.167s+1)(.0111s+1)}\ (\text{rad/rad})$$

θ = fuselage slope at Sta. 47

Wing Rotation (δ_w) due to Vertical Acceleration ($\ddot{z}$)

$$\delta_w(\text{deg}) = k_{\ddot{z}}\left(\frac{\bar{s}}{\bar{s}+0.1}\right)\left(\frac{30}{\bar{s}+30}\right)\ddot{z}\ (\text{in/sec}^2)$$

$$s = \frac{\bar{s}}{3}$$

$$\frac{\delta_w}{z} = \frac{.006464k_{\ddot{z}}s^3}{(3.33s+1)(.0111s+1)}\ (\text{rad/in})$$

z = the vertical displacement of the fuselage at Sta. 47.

The "basic" values of constants are:

$k_{\dot{\theta}} = .262$

$k_{\ddot{z}} = 6.477 \times 10^{-4}$

Stability Analysis Summary

Case	Run	V knots	SAS $k_{\ddot{z}}$	SAS $k_{\dot{\theta}}$	Stiffness factor	Description
5	1	-	--	--	x1	Normal Modes
5	2	100	0	0	x1	Flutter Analysis
5	3	200	0	0	x1	" "
5	4	300	0	0	x1	" "
17	1	170.7	0	0	x1	Stability of
15	1	170.7	0	.262	x1	flexible airplane
15	2	170.7	$6.477\text{x}10^{-4}$	.262	x1	varying $k_{\ddot{z}}$
18	1	170.7	$6.477\text{x}10^{-3}$	.262	x1	
18	2	170.7	.06477	.262	x1	
20	1	170.7	$6.477\text{x}10^{-4}$	.262	x1000	Stability of
20	2	170.7	$6.477\text{x}10^{-3}$	.262	x1000	stiff airplane
20	3	170.7	.06477	.262	x1000	varying $k_{\ddot{z}}$
16	1	170.7	$-6.477\text{x}10^{-4}$	.262	x1	Stability with $k_{\ddot{z}}$ sign inversion

Frequency Response Gust Analysis

The gust spectrum used is given by

$$\Phi(\omega) = \frac{.06}{4x10^{-6}+(\omega/U)^2} \text{ (ft/sec)}^2\text{/rad/ft}$$

The gust analysis was performed for an airplane velocity (U) of 170.7 knots. The table of gust velocity (V_g) versions of frequency (f) used in the analysis was calculated from

$$V_g(f) = \frac{.96511}{8.4224x10^{-3}+f^2} \text{ knots}/\sqrt{\text{hz}}$$

The printed or plotted output from SADSAM will bear dimensions of

$$\text{output units}/\sqrt{\text{hz}} \quad .$$

For example accelerations, scaled in SADSAM to units of g, will be in units of

$$\text{g's}/\sqrt{\text{hz}} \quad .$$

The mean square value, calculated by SADSAM for any output quantity, ϕ, is given by

$$MS = \int_{f_1}^{f_n} \phi^2 df$$

The mean square value of an acceleration output request scaled to g's then has units of g^2.

Run Description

Case 21 Run 1 Flexible airplane, with SAS
Case 21 Run 2 Flexible airplane, without SAS
Case 21 Run 3 Airplane 1000x stiffer, with SAS
Case 21 Run 4 Airplane 1000x stiffer, without SAS

Output Summary

Case 21

Run No.		1	2	3	4
Flex/Stiff		Flex	Flex	Stiff	Stiff
SAS		Yes	No	Yes	No
Mean Square Values					
A22	$\ddot{z}$ near airplane CG $(g)^2$	.07566	.08063	.05193	.05691
A56	$\ddot{z}$ at root of horiz. tail $(g)^2$	.8033	.7526	.3535	.3819
A2	$\ddot{z}$ at wing tip $(g)^2$	1.3967	1.3745	.05152	.05647
A71	$\ddot{z}$ at tip of horiz tail $(g)^2$	1.1744	1.2087	.3530	.3814
A24	$\ddot{\theta}$ at root of wing $(rad/in)^2$	.1256E-4	.1136E-4	5.844E-6	6.056 E-6
A58	$\ddot{\theta}$ at root of horiz tail $(rad/in)^2$	2.463 E-4	1.986 E-4	.1314E-4	6.059 E-4
E4	wing root bending moment $(in\ lb)^2$	4.593 E8	4.893 E8	3.481 E8	3.633 E8
E28	horiz tail root bending moment $(in\ lb)^2$	2.567 E6	1.950 E6	1.149 E6	.9775 E6
E18	fuselage bending moment aft of wing $(in\ lb)^2$	.1161E8	7.902 E6	9.858 E6	7.327 E6
E20	fuselage bending moment forward of tail $(in\ lb)^2$	3.703 E6	2.524 E6	2.179 E6	1.693 E6
E14	wing root torsion $(in\ lb)^2$	.4120E6	.4692E6	.3154E6	.3781E6
E34	tail root torsion $(in\ lb)^2$	.3430E4	.2318E4	.1184E4	778.3
F7	gust load on wing cell $(lb)^2$	6.322 E4	6.322 E4	6.322 E4	6.322 E4
F66	gust load on tail cell $(lb)^2$	.7351E4	.7351E4	.7351E4	.7351E4

Case 21	Run 1	2	3	4
RMS Values				
A22	.2751	.2840	.2279	.2386
A56	.8963	.8675	.5946	.6180
A2	1.1818	1.1724	.2270	.2376
A71	1.0837	1.0994	.5941	.6176
A24	3.544 E-3	3.370 E-3	2.417 E-3	2.461 E-3
A58	15.69 E-3	14.09 E-3	3.625 E-3	2.462 E-3
E4	21431	22120	18657	19060
E28	1602	1396	1072	989
E18	3407	2811	3140	2707
E20	1924	1589	1476	1301
E14	641.9	685.0	561.6	614.9
E34	58.57	48.15	34.41	27.90
F7	251.4	251.4	251.4	251.4
F66	85.74	85.74	85.74	85.74

RMS Ratio

	with SAS/without SAS		FLEX/STIFF	
	FLEX	STIFF	SAS	No SAS
A22	.9687	.9552	1.207	1.190
A56	1.0332	.9621	1.507	1.404
A2	1.0080	.9554	5.206	4.934
A71	.9857	.9619	1.824	1.780
A24	1.0516	.9821	1.466	1.369
A58	1.1136	1.4724	4.328	5.723
E4	.9689	.9789	1.149	1.161
E28	1.1476	1.0839	1.494	1.412
E18	1.2120	1.1600	1.085	1.038
E20	1.2108	1.1345	1.304	1.221
E14	.9371	.9133	1.143	1.114
E34	1.2164	1.2333	1.702	1.726
F7	1.0	1.0	1.0	1.0
F66	1.0	1.0	1.0	1.0

Transient Gust Analysis

Airplane velocity = 170.7 knots

Sharp Edge Gust

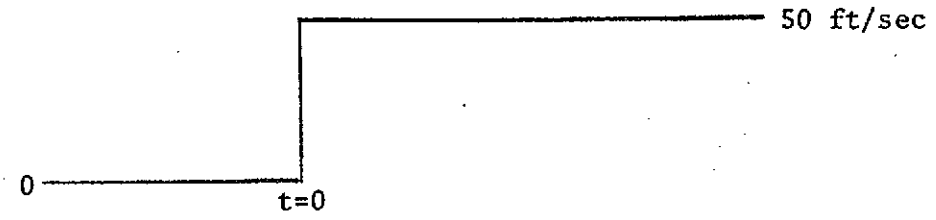

Case 23 - no structural damping

Run 1 flexible airplane with SAS

Run 2 flexible airplane without SAS

Run 3 1000x stiffer airplane with SAS

Run 4 1000x stiffer airplane without SAS

Case 24 - structural damping added by means of SIMDAMP card in SADSAM, where g = .01 at 20 hz. Run schedule same as Case 23 above.

Transient Output

Same as frequency response solutions plus:

V22 vertical velocity near airplane CG (in/sec)

D39 pitch slope displacement of fuselage near the airplane CG (rad)

General Notes:

Consistent plotting scales between runs were accomplished for the frequency response solution by repeating the entire solution and specifying the plot scales chosen from a prior solution. This same task could be, but was not accomplished for the transient solution.

Case 24 (transient solution) was performed with a small amount of structural damping. Case 23 was run with no damping and resulted in generally "noisy" solutions and in run 1, a high frequency instability. This high frequency solution content is probably the result of the numerical integration destabilizing some marginally stable high frequency root of the system. It is recommended that some structural damping be included in all transient solutions. Case 23 is included here to demonstrate that even the small damping included in Case 24 (g = .01 at 20 cps) can have a profound effect.

It should be noted that the gust loads on the horizontal tail are delayed .05 seconds after the gust loads on the wing. The effect of this delay can be seen in most of the plotted output and is most evident in the plots of F66, the gust load on a tail strip. In the frequency response solution the phase plot of F66 shows approximately a linearly increasing phase angle with frequency. The transient solution plot shows a .05 second delay before the onset of the load at F66.

The transient solution converges to a constant angle of attack, equal and opposite to the gust angle (.1734 rad).

Case 24 t = 1.0 seconds

Run	V22 in/sec	D39 rad	V22 knots	n/v V22/170.7 rad	$\bar{\alpha}$ θ - n/v
1	228.92	-.1070	11.295	.0662	-.1732
2	122.87	-.1380	6.062	.0355	-.1735
3	231.80	-.1062	11.437	.0670	-.1732
4	128.78	-.1363	6.354	.0372	-.1735